WOOD RESEARCH
51 (3): 2006
11-24

NON-DESTRUCTIVE TESTING OF TRUNKS: STUDYING ELASTIC WAVE PROPAGATION BY NUMERICAL SIMULATION

Sandy Schubert
EMPA / ETH Zürich, Switzerland

Daniel Gsell, Masoud Motavalli
EMPA, Zürich, Switzerland

Jürg Dual, Peter Niemz
ETH, Zürich, Switzerland

ABSTRACT

Visual tree assessment (VTA) is carried out to evaluate the stability of urban trunks. For identification of fungal decay non-destructive methods, based on elastic wave propagation, are used to supplement VTA. This study aims at a profound understanding of the wave propagation phenomena in the radial-tangential plane of a trunk with the intention of enhancing those methods for identification of decay.

The simulation model is described in detail. Since no closed form analytical solution of this propagation problem exits, numerical simulation based on the finite-difference-time domain method (FDTD) is used. Thus, a two-dimensional cylindrical FDTD code is developed, which represents the cylindrical cross-section and considers the anisotropy of wood. The characteristics of wave propagation in the anisotropic material are studied by a "healthy" reference model using snapshots of the displacement amplitudes at different propagation times. The influence of fungal decay is investigated for two different sizes of decayed regions (5% and 11% of the total area) and two different degrees of decay: total degradation of the wood (cavity) and reduced wave velocities (75%). Subsequently these results are compared with the influence of a heterogeneous distribution of density and different moisture content.

The anisotropy of the material results in a characteristic wavefront of the P-wave. The influence of size and degree of decay is significant in the synthetic data. However, the uncertainties according to the natural grown material wood and to the measurement system require a robust and over-determined data processing algorithm to interpret the travel-times.

KEY WORDS: non-destructive testing, numerical simulation, fungal decay, wave propagation, FDTD, Visual Tree Assessment (VTA)

INTRODUCTION

In the urban environment trees are frequently exposed to hostile environmental conditions. These endanger the street trees more than others to development of decay or formation of structural defects. Stability loss or breakage of branches may be caused by those and lead to hazards to life or property. Hence, maintenance is carried out by the municipalities. The visual tree assessment (VTA) includes estimating vitality, injuries and illnesses of the tree leading to the final evaluation of its stability. Though, the degradation of wood inside the trunk, due to rot fungus, is impossible to estimate visually from the outside. Thus, destructive methods for investigating the trees are used: drill resistance measurements and the removal and assessment of a drilling core. Since injuring the tree opens up possibilities for new fungal pathogens to invade the trunk, nondestructive testing methods are preferable. Today, the methods used therefore are based on elastic waves. The influence fungal decay has on elastic wave propagation results from its effects on density, stiffness and moisture content. As many parameters influence the wave propagation phenomena, the most important ones are summarized in Fig. 1.

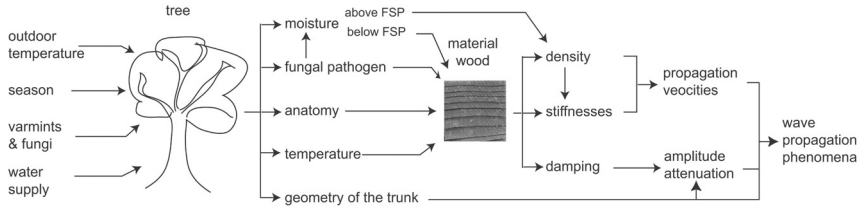

Fig. 1: Important influence factors on the wave propagation phenomena

The anatomical structure of wood determines intrinsically its properties: density, stiffness and damping. The propagation velocities of the elastic waves are determined by stiffness and density. The geometrical spreading of the wavefront and the damping influences significantly the attenuation of the wave amplitudes. Wave propagation phenomena are determined by stiffness, density, damping and geometry of the trunk. A fungal pathogen can degrade wood constituents and influence the moisture transport in the material. If this results in distinguishable material properties of sound and decayed wood the fungus influences the propagation phenomena. The nondestructive methods based on elastic waves use different approaches: impact-hammer excitation and excitation with piezo-electric transducers are common, the frequency ranges from 100Hz -3kHz and 10kHz -50kHz, respectively. The traveltime of the P-Wave is measured and the corresponding velocities are interpreted by comparing with literature values. A more sophisticated approach regarding data-processing is used by Socco et al. (2004), where an inversion algorithm is applied to carry out traveltime tomography. This algorithm was developed for seismic investigations in isotropic media and does not take into account the anisotropy of the material wood.

The wave propagation phenomena in the anisotropic, natural material are very complex. Thus the measurements can only be understood if the physical background is considered and appropriate assumptions and simplifications are applied to the simulation model for studying propagation phenomena. In this work a simplified trunk model is presented and an appropriate simulation method is applied to study the wave propagation phenomena in respect to:

• the anisotropic material behavior
• different stages and sizes of fungal decay
• density distributions (circular) of the material
• varying moisture content

This work aims at a better understanding of the traveltime measurements. Moreover, synthetic data for in-depth testing the quality and potential of traveltime tomography is available.

For the propagation of elastic waves in anisotropic media with curved boundaries no closed form analytical solution exits. Hence, the problem is solved numerically. The most common modelling technique for wave-propagation phenomena is the finite-differencetime-domain method (FDTD), which is used in this project. The wooden trunk can be described as an orthotropic material with respect to the cylindrical coordinate system. Gsell et al. (2004) describes the tree-dimensional elastic wave propagation in anisotropic, cylindrical shells. Whereas Chen et al. (1998) provides an example of a three-dimensional cylindrical FDTD code for an isotropic medium. In this work a two-dimensional cylindrical FDTD code for the plain-strain state is developed. This approach is sufficient since the main objectives are: explanation of traveltime measurements and the propagation phenomena in principle. Furthermore, the orthotropic material behavior and the heterogeneity due to centered fungal degradation is considered.

Trunk model

The simulation model of the trunk is an idealization of real trunks. For a reasonable characterization of the wave propagation phenomena in trunks it is necessary to apply appropriate simplifications and to take in account the important properties. In the described model the following properties are considered:

• cylindrical orthotropic behavior of wood
• circular shaped heterogeneity of material properties

As it is shown in the comparison with an isotropic model, the cylindrical orthotropic behavior of wood influences the wave propagation significantly. It is described by the linear elastic material law of Hooke,

$$\begin{bmatrix} \sigma_{ll} \\ \sigma_{rr} \\ \sigma_{\varphi\varphi} \\ \sigma_{r\varphi} \\ \sigma_{l\varphi} \\ \sigma_{lr} \end{bmatrix} = \begin{bmatrix} C_{11} & C_{12} & C_{13} & 0 & 0 & 0 \\ C_{21} & C_{22} & C_{23} & 0 & 0 & 0 \\ C_{31} & C_{32} & C_{33} & 0 & 0 & 0 \\ 0 & 0 & 0 & C_{44} & 0 & 0 \\ 0 & 0 & 0 & 0 & C_{55} & 0 \\ 0 & 0 & 0 & 0 & 0 & C_{66} \end{bmatrix} \begin{bmatrix} \epsilon_{ll} \\ \epsilon_{rr} \\ \epsilon_{\varphi\varphi} \\ 2\epsilon_{r\varphi} \\ 2\epsilon_{l\varphi} \\ 2\epsilon_{lr} \end{bmatrix}. \tag{1}$$

Where σ are the stresses, ε the strains and C the orthotropic stiffness tensor with nine independent elements. The definitions of the coordinate system of the trunk are depicted in Fig. 2. Since the main interest is to study the general wave-propagation phenomena in the trunk, following simplifications are assumed for the model:

1. ideal circular crossection (Fig. 2)
2. mark in the center of the crossection
3. reduction to a two dimensional problem

Whereas the 2D approach, modelling the radial-tangential plane of the trunk, is sufficient for studying the arrivals of the different wave-types. Mainly, the first arrivals of the fastest wave (P-wave) are of interest. For the case of plane waves the velocity for the P-wave in radial v_{P_r} and

tangential direction v_{Pt} are defined by the elements of the stiffness tensor (C_{22}, C_{33}) and the density ρ,

$$v_{Pr} = \sqrt{\frac{C_{22}}{\varrho}}, \quad v_{Pt} = \sqrt{\frac{C_{33}}{\varrho}}. \tag{2}$$

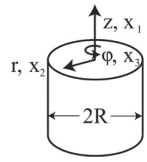

Fig. 2: Definition of the coordinate system

The size of the microscopical elements of the wood structure -the cells -are in the µmrange and of the macroscopical growthrings are in the range of ≈ 1 – 3mm. Since the wavelength in the investigated frequency range 10kHz–50kHz amounts to ≈ 15cm–3cm, the material is assumed to be homogeneous.

Theoretical background

The equilibrium conditions in cylindrical coordinates (Graff 1991, Rose 1999) for the plane-strain deformation state are given as

$$\varrho \frac{\partial^2 u_r}{\partial t^2} = \frac{\partial \sigma_{rr}}{\partial r} + \frac{1}{r}\frac{\partial \sigma_{r\varphi}}{\partial \varphi} + \frac{\sigma_{rr} - \sigma_{\varphi\varphi}}{r}, \tag{3}$$

$$\varrho \frac{\partial^2 u_\varphi}{\partial t^2} = \frac{\partial \sigma_{r\varphi}}{\partial r} + \frac{1}{r}\frac{\partial \sigma_{\varphi\varphi}}{\partial \varphi} + \frac{2\sigma_{r\varphi}}{r}, \tag{4}$$

with u_r and u_φ the displacement components, σ_{rr} and $\sigma_{\varphi\varphi}$ the normal stresses, $\sigma_{r\varphi}$ the shear stress and the density ρ. The relations between the stresses σ and the strains $\in$ of linear elastic anisotropic material are described by the elastic stiffness tensor C inEq. 1 (Noack and Roth 1976) rhombic and cylindrical orthotropic wood. Regarding the plain-strain deformation state in the radial-tangential plane, the strains $\in_{zz}$, $\in_{rz}$, $\in_{\varphi z}$ and the stresses σ_{rz}, $\sigma_{\varphi z}$ vanish. Yielding the following stress-strain relations for the orthotropic material wood in the "ideal" trunk

$$\begin{bmatrix} \sigma_{rr} \\ \sigma_{\varphi\varphi} \\ \sigma_{r\varphi} \end{bmatrix} = \begin{bmatrix} C_{22} & C_{23} & 0 \\ C_{32} & C_{33} & 0 \\ 0 & 0 & 2C_{44} \end{bmatrix} \begin{bmatrix} \epsilon_{rr} \\ \epsilon_{\varphi\varphi} \\ \epsilon_{r\varphi} \end{bmatrix} \tag{5}$$

Where the strains are derived from linear kinematic relations in cylindrical coordinates

$$\epsilon_{rr} = \frac{\partial u_r}{\partial dr}, \tag{6}$$

$$\epsilon_{\varphi\varphi} = \frac{u_r}{r} + \frac{1}{r}\frac{\partial u_\varphi}{\partial \varphi}, \tag{7}$$

$$\epsilon_{r\varphi} = \frac{1}{2}\left(\frac{1}{r}\frac{\partial u_r}{\partial d\varphi} + \frac{\partial u_\varphi}{\partial r} - \frac{u_\varphi}{r}\right). \tag{8}$$

Numerical method

Discretization

To obtain a numerical solution of the wave-propagation problem, Eqs. 3 to 8 were discretized using central differences with staggered grids (Figure 3) first introduced by Yee (1966). The discretizised forms Eq. 3 and Eq. 4 are,

$$\begin{aligned}\varrho\frac{({}^{new}u_r - 2u_r + {}^{old}u_r)^{(j,k)}}{dt^2} &= \frac{\sigma_{rr}^{(j+1/2,k)} - \sigma_{rr}^{(j-1/2,k)}}{\Delta r} + \frac{\sigma_{r\varphi}^{j,k+1/2} - \sigma_{r\varphi}^{(j,k-1/2)}}{\Delta\varphi R^{(j)}} \\ &\quad + \frac{\sigma_{rr}^{(j+1/2,k)} + \sigma_{rr}^{(j-1/2,k)}}{2R^{(j)}} - \frac{\sigma_{\varphi\varphi}^{(j+1/2,k)} + \sigma_{\varphi\varphi}^{(j-1/2,k)}}{2R^{(j)}}\end{aligned} \tag{9}$$

$$\begin{aligned}\varrho\frac{({}^{new}u_\varphi - 2u_\varphi + {}^{old}u_\varphi)^{(j+1/2,k+1/2)}}{dt^2} &= \frac{\sigma_{r\varphi}^{(j,k+1/2)} - \sigma_{r\varphi}^{(j+1,k+1/2)}}{\Delta r} \\ &\quad + \frac{\sigma_{\varphi\varphi}^{(j+1/2,k+1)} - \sigma_{\varphi\varphi}^{(j+1/2,k)}}{\Delta\varphi R^{(j+1/2)}} + \frac{\sigma_{r\varphi}^{(j,k+1/2)} + \sigma_{r\varphi}^{(j+1,k+1/2)}}{R^{(j+1/2)}}.\end{aligned} \tag{10}$$

where ${}^{new}u_i$ denotes the value of u_i in the following timestep and ${}^{old}u_i$ of the last. The values for the current timestep are without left index. Eq. 6 to Eq. 8 are inserted in Eq. 5. Using central differences the discretizised stress-displacement relations are derived,

$$\begin{aligned}\sigma_{rr}^{(j+1/2,k)} &= C_{22}\frac{u_r^{(j+1,k)} - u_r^{(j,k)}}{\Delta r} \\ &\quad + C_{23}\left(\frac{u_r^{(j+1,k)} + u_r^{(j,k)}}{2R^{(j+1/2)}} + \frac{u_\varphi^{(j+1/2,k+1/2)} - u_\varphi^{(j+1/2,k-1/2)}}{\Delta\varphi R^{(j+1/2)}}\right),\end{aligned} \tag{11}$$

$$\begin{aligned}\sigma_{\varphi\varphi}^{(j+1/2,k)} &= C_{32}\frac{u_r^{(j+1,k)} - u_r^{(j,k)}}{\Delta r} \\ &\quad + C_{33}\left(\frac{u_r^{(j+1,k)} + u_r^{(j,k)}}{2R^{(j+1/2)}} + \frac{u_\varphi^{(j+1/2,k+1/2)} - u_\varphi^{(j+1/2,k-1/2)}}{\Delta\varphi R^{(j+1/2)}}\right)\end{aligned} \tag{12}$$

$$\begin{aligned}\sigma_{r\varphi}^{(j,k+1/2)} &= C_{44}\frac{1}{2}\left(\frac{u_r^{(j,k+1)} - u_r^{(j,k)}}{\Delta\varphi R^{(j)}}\right., \\ &\quad \left. + \frac{u_\varphi^{(j+1/2,k+1)} - u_\varphi^{(j+1/2,k)}}{\Delta r} - \frac{u_\varphi^{(j+1/2,k+1)} + u_\varphi^{(j+1/2,k)}}{2R^{(j)}}\right).\end{aligned} \tag{13}$$

In Fig. 3 the distribution of deformation and stress components are depicted. The center of the cell (*j, k*) is located at

$$\begin{aligned} r_j &= r_{min} + (\frac{1}{2} + j)\Delta r, \\ \varphi_k &= (\frac{1}{2} + k)\Delta\varphi. \end{aligned}$$

The radius r_{min} is determined by Δr as the boundary conditions require $r_{min} > \Delta r/2$. Due to the reciprocal value of the radius in the FDTD code there is a singularity in the center of the grid. Therefore the center is treated as a small hole with free boundary. This hole does not influence the wave significantly, if it is small in comparison to the wavelength.

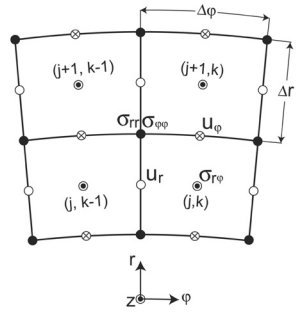

Fig. 3: Staggered grid with cell numbering, displacements u and stresses σ

Boundary conditions

The boundary conditions at the inner radius r_{min} are assumed to be stress-free. At the outer radius *R* the surface is stress-free or a stress component is applied in the radial direction at the excitation points. The boundary conditions are implemented by introducing a fictitious layer next to the surface as described in Gsell et al. (2004). The required fictitious values $\hat{\sigma}_{r\varphi}$ and $\hat{u}_r$ are calculated

$$\begin{aligned} \hat{\sigma}_{r\varphi}^{(k)} &= -\sigma_{r\varphi}^{(J,k)}, \\ \hat{u}_r^{(k)} &= \left[\sigma_{rr}^{(J,k)} - \frac{C_{23}}{R^{(J+1/2)}}\frac{\partial u_\varphi^{(J,k)}}{\partial\varphi} - u_r^{(J,k)}\left(\frac{C_{23}}{2R^{(J+1/2)}} - \frac{C_{22}}{\Delta r}\right)\right] \Big/ \left(\frac{C_{23}}{2R^{(J+1/2)}} + \frac{C_{22}}{\Delta r}\right), \end{aligned}$$

with *J* number of elements in radial direction and the radial stress component on the surface $\sigma_{rr}^{J,k}$

$$\sigma_{rr}^{(J,k)}(t) = \begin{cases} 0, & \text{free surface} \\ s(t), & \text{excitation} \end{cases} \tag{14}$$

with *s*(*t*) the signal of the excitation. Hence, the stress and deformation components on the surface $\sigma_{\varphi\varphi}^{J,k}$ and $u_\varphi^{J,k}$ are calculated using the fictitious values $\hat{u}_r$ and $\hat{\sigma}_{r\varphi}$, respectively.

Sampling rate and timestep

The size of the cells influences the numerical dispersion. Therefore, the wavelength λ of the P-wave in radial direction is sampled more than 20 times,

$$\Delta r \leq \frac{\lambda}{20}, \quad \text{with } \lambda = \frac{v_{Pr}}{f_{max}}, \tag{15}$$

The timestep Δt is chosen according to Chen et al. (1998)

$$\Delta t \leq \frac{1}{v_{Pr}\sqrt{(\Delta r)^{-2} + (r_{min}\Delta\varphi(r_{min}))^{-2}}}, \tag{16}$$

to assure the stability of the simulation.

RESULTS AND DISCUSSION

In opposite to the measurements on trunks, the described simulation model gives the opportunity to study the influence of parameters separated. The aim of this parameter study is to verify and estimate the influence of fungal decay on wave propagation in comparison to: (1) anisotropy, (2) heterogeneous distribution of density and (3) different moisture distributions. With regard to the signal processing of the measurement data, the parameter study focusses on the first arrival of the P-wave.

Reference model

The influence of the several parameter on the wave propagation is estimated relative to the reference model. This model has a diameter of D = 45cm and a homogenous density and stiffness distribution, the used values are summarized in Tab. 1. The density ρ_{40} was calculated for spruce(*Picea abies*) with a dry density ρ_{dr} = 420kg/m^3 and a moisture content MC = 40%. The excitation of the elastic wave was introduced by normal stress $\sigma_{rr} = s(t)$ applied to a part of the surface with a width of 1.5cm. The signal $s(t)$ is depicted in Fig. 4.

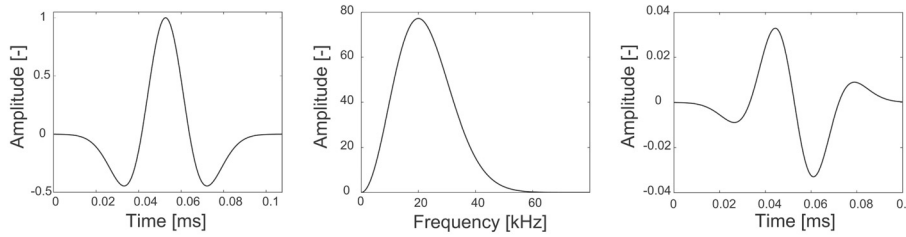

Fig. 4: Signal s(t) used for the excitation (left), its frequency spectrum (middle) and its first derivative (right)

All described models have a diameter of D = 45cm. As excitation, the signal s(t) of Fig. 4 is used.

Comparison of wave propagation in isotropic and anisotropic models

Comparing wave propagation phenomena in a anisotropic and a fictitious isotropic trunk highlights the complex anisotropic behavior. Isotropic material is characterized by its P-and S-wave velocity v_P and v_S. The material properties for the corresponding isotropic model are defined by the properties of the reference model (index *ref*). Due to the P- and S-wave velocity $v_P = v_{Pr}$ = 1482m/s and $v_S = \sqrt{C_{44}^{ref}/\rho^{ref}}$ = 250m/s the other properties are given (Tab. 1).

Tab. 1: Material properties of the reference and the isotropic model

model	ρ_{40} kg/m^3	C_{22} N/mm^2	C_{33} N/mm^2	C_{23} N/mm^2	C_{44} N/mm^2
reference	546	1200	600	300	34
isotrop	546	1200	1200	1130	34

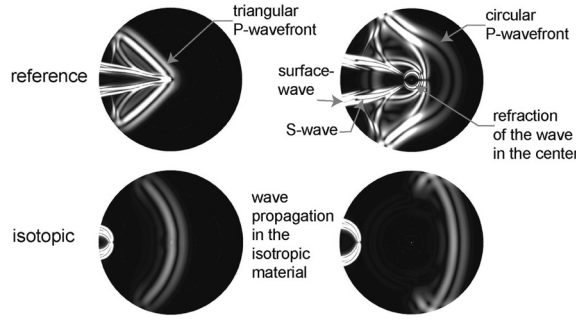

Fig. 5: Comparison of the wave propagation phenomena in isotropic and cylindrical anisotropic material; absolute displacements for 0.22 ms and 0.30 ms after excitation start; black: small amplitudes; white: large amplitudes

The three main differences between the propagation phenomena depicted in Fig. 5 are:

- The first wavefront in the anisotropic model is triangular in front of the center and circular with radius $R = D/2$ behind, the isotropic model is always circular with a radius $R > D/2$. This is caused by the different stiffness and corresponding wave velocities in radial and tangential direction.
- The fastest wave is slower in the anisotropic than in the isotropic model, despite that the velocities of plane P-wave propagation are equal in both materials. This difference is caused by different poisson ratios.
- The wave refraction in the center of the anisotropic model is caused by the unsteady change of the material properties in the center.

The first two differences are highlighted in the velocity diagram, which is later used again for showing the influence of fungal decay. In this diagram the average velocities v of the wave between point A and B are calculated by $v = s_{ab}/t_{ab}$ with s_{ab} the distance and t_{ab} the travel time between A and B. The velocities of the two models between point A, the excitation point, and

the points B_i, the "measurement points", are depicted in Fig. 7 (left). The measurement points B_i are located on the surface of the trunk and their position is defined by the angle Θ, (Fig. 6). The first-break onsets of the synthetic data are determined using a picking algorithm based on the AIC criteria (Zhang et al. 2003)

$$AIC(w(t_m)) = m \log\{\mathrm{var}(w[1, m])\} + (N - m - 1) \log\{\mathrm{var}(w[m+1, N])\}. \quad (17)$$

Therefore the part of the signal *s(t)* containing its onset: *w(t)* is chosen manually. *N* is the length of *w(t)* and t_m the time at step *m*. The variance var(*w*[*a*, *b*]) is calculated by

$$\mathrm{var}(w[a,b]) \;=\; \frac{1}{b-a}\sum_{i=a}^{b}(w(t_i) - \overline{w})^2, \quad (18)$$

with $\overline{w}$ the mean value of *w*(*t*). The onset is defined by the minimum of the AIC criteria *AIC*(*w*(*t*)).

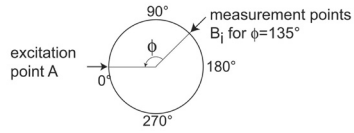

Fig. 6: position of measurement points on the surface

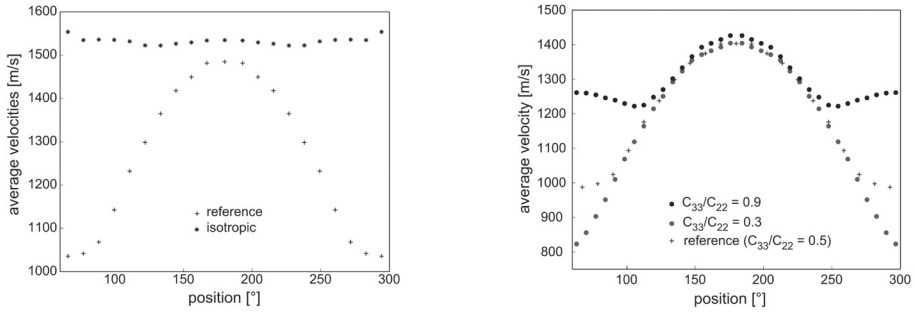

Fig. 7: Average velocities for the arrival of the P-wave on the surface; comparison between isotropic and anisotropic model (left), varying ratios C_{33}/C_{22} (right)

The ratio of tangential and radial stiffness C_{33}/C_{22} is a degree for the anisotropy, as the ratio is 1 for isotropic material. In Fig. 7 (right) is the influence of the ratio between tangential and radial stiffness obvious. For the calculation of the models C_{33}/C_{22} =0.9 and C_{33}/C_{22} =0.3 a sinusoidal excitation of 20kHz is used. The stiffness in radial direction C_{22}, C_{44} und C_{23} are equal to the reference model. Analog to stiffness the velocities are varied υ_{Pr} and υ_{Pt} (Eq. 2): υ_{Pr} is equal, $v_{Pt} = 180\% v_{Pt}^{ref}$ (C_{33}/C_{22} =0.9) and $\upsilon_{Pt} = v_{Pt} = 60\% v_{Pt}^{ref}$ (C_{33}/C_{22} =0.3). This change in the propagation velocities in tangential direction υ_{Pt} results in changing average velocities in the region of $0° \le \theta \le 120°$ and $240° \le \theta \le 360°$.

Fungal decay

The influence of fungal decay is studied for two different sizes of decayed regions, 5% and 11% of the total area of the trunk cross-section, and for two different degrees of decay: total degradation of the wood (cavity), reduced stiffness (50%) and density (88%), i.e. 75% of the P-wave velocity. These values are according to experiments with laboratory decayed wood, described in Schubert et al. (2006). The specimens (Norway spruce) showed after 8 weeks of inoculation with *Ganoderma lipsiense* a maximal decrease of 50% stiffness, when the density decreased 12%. The parameters of the four models are summarized in Tab. 2, where r_f stands for the radius of the decayed region.

Tab. 2: Material properties for models 1 to 4

nr.	d_f cm	d_f /D %	degree of decay	ρ_{40} kg/m^3	C_{22} N/mm^2	C_{33} N/mm^2	C_{23} N/mm^2	C_{44}
1	10	22	cavity	-	-	-	-	-
2	15	33	cavity	-	-	-	-	-
3	10	22	medium	480	600	300	150	17
4	15	33	medium	480	600	300	150	17
reference	-	-	-	546	1200	600	300	34

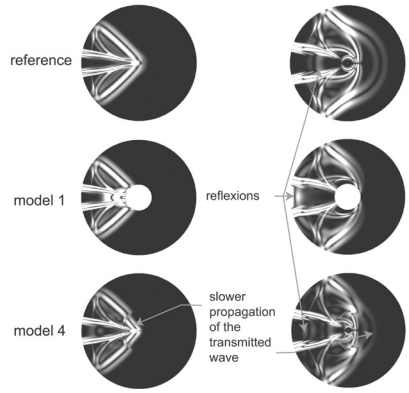

Fig. 8: Comparison of the wave propagation phenomena in the reference model and two of the fungal decay models: cavity of 5% and medium degree of fungal decay of 11%; absolute displacements for 0.22 ms and 0.30 ms after the excitation started; black: small amplitudes; white: large amplitudes

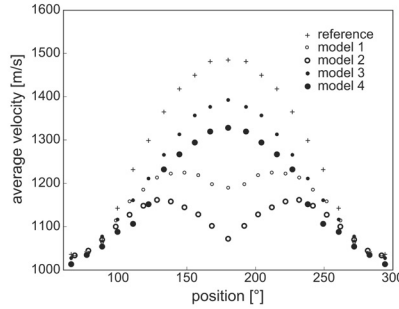

Fig. 9: Average velocities for the arrival of the P-wave on the surface; comparison between reference and model 1 to 4

The propagation phenomena of model 1 and 2 are depicted in Fig. 8. The results of the comparison between the model 1 to 4 and the reference model showed in Fig. 9 are summarized:

- The P-wave is reflected at the boundary of the decayed area.
- The characteristic curve of the velocities (Fig. 9) changes for models with cavities(o), but not for models with reduced (50%) stiffness (•).
- The velocity decreases with increase of the area of fungal decay.
- The velocity decreases with increase of the degree of fungal decay.

Heterogenous distribution of density and varying moisture content

The heterogeneity of density and stiffness of the wood have many reasons, e.g. compression wood or circular changes due to the age of the tree. Latter are studied in Model 5 and 6 (Fig. 10) with three parts of different densities are compared to the reference model. Whereas one model has the same average density ρ as the reference density ρ^{ref} and the other has $0.75\rho^{ref}$ resulting in a higher velocity. Additionally, the influence of the moisture content (MC) was studied with model 7 (Fig. (left)), in which for the sapwood a MC of 145% and for the heartwood of 46% is assumed. The corresponding densities are calculated on base of a dry density of ρ_{dr} = 420kg/m^3.

The results for the three models are depicted in Fig. 11. It is obvious, that there is no change in the characteristic shape of the curve and mainly the higher average density value is responsible for the differences between reference and model 6 and 7.

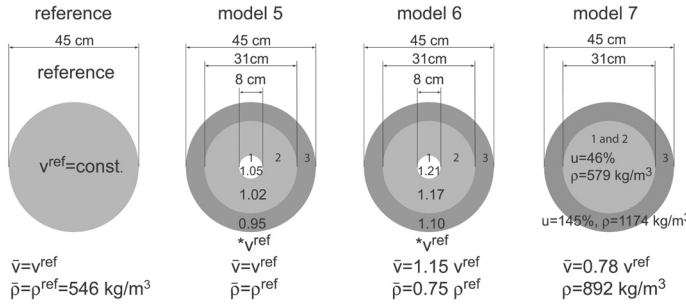

Fig. 10: Density distribution for model 5 and 6

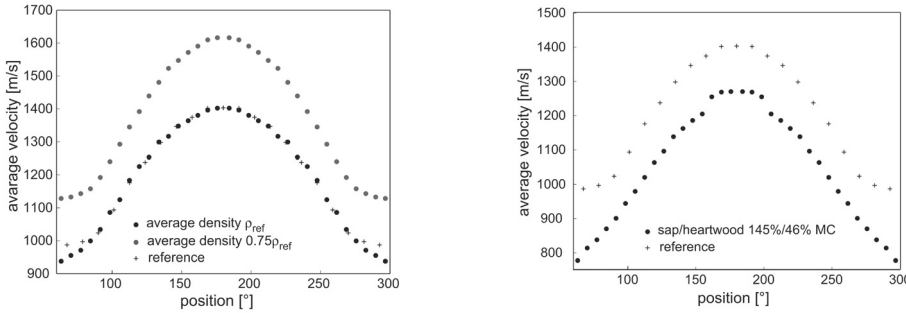

Fig. 11: Material properties of model 7 (left). Average velocities for the arrival of the P-wave on the surface; comparison between reference and model 5 and 6 (left), reference and model 7 (right)

CONCLUSSIONS

The numerical simulation visualizes the wave propagation in the radial-tangential trunk-plane of trees and yields a better understanding of the phenomena. The wavefront of the P-wave is observed to be triangular before reaching the center. Behind the center it propagates in the radial direction. Therefore, its front has a circular shape. This characteristic phenomena is explained by the cylindrical anisotropy of the wood and Fermat's principle, which requires that the P-wave travels along the fastest path. The wavefront shape of the reference model is validated in Maurer et al. (2005) using traveltime computation described in Faria and Stoffa (1994). The calculated traveltime isochrones show the same characteristic as the wavefront in the simulation. Additionaly, both the wavefront shape and the refraction of the P-wave in the center are observed in the semi-analytical solution of Payton (2003). There, the wave fronts of the P and S-Wave in an unbounded cylindrical anisotropic medium, are calculated for an example with wood properties.

The wave propagation in the radial-tangential plane is a complex phenomenon even in the "ideal" trunk. It has been shown, that a circular heterogenous distribution of the density does not influence the shape of the velocity curve, (Fig. 11). Looking at the average velocities for the different models, the influence of size and degree of decay is obvious in the synthetic data. In contrast, the interpretation of the measurement data implies several additional difficulties:

1. Variation of the global material parameters of wood ⇒ unknown reference values.
2. The time delay of the measurement system is unknown ⇒ underestimation of the average velocities and change of the characteristic shape.
3. Irregularities in the wood like branches, non-cylindrical anisotropy etc. ⇒ change of the characteristic shape of velocity versus position for "healthy" trees.
4. Uncertainty of the distance between position of excitation and measurement ⇒ inaccuracy of the average velocity calculation.

The first problem can be solved by reference measurements on other locations of the trunk. Calibrating the system before the measurement minimizes the time delay mentioned in the second item. According to items 2. to 4. the interpretation of the average velocity plots may lead to a wrong assessment. Thus, a more robust and over-determined data processing algorithm like in Socco et al. (2004) is necessary. The traveltime tomography algorithm has been improved by Maurer et al. (2005) for the anisotropy of the trunk and tested with synthetic data of the simulation model proposed in this work. Further investigations might be focused on improved inversion algorithms including the shape of measured signals and studying the reliability of the signal processing in respect of non-circular heterogeneities and crossections with the mark not centered.

REFERENCES

1. Chen, Y. H. et al., 1998: A three-dimensional finite difference code for the modeling of sonic logging tools. Journal of the Acoustical Society of America 103(2): 702-712
2. Faria, E.L., Stoffa, P.L., 1994: Traveltime computation in transversely isotropic media. Geophysics 39(2):272-281
3. Graff, Karl F., 1991: Wave Motion in Elastic Solids. Dover Publications. New York
4. Gsell, D. et al., 2004: Modeling three-dimensional elastic wave propagation in circular cylindrical structures using a finite-difference approach. Journal of the Acoustical Society of America 116(6): 3284-3293
5. Langenberg, K. J. et al.,2000: Application of modeling techniques for ultrasonic austenitic weld inspection. NDT & E international 33: 465-480
6. Maurer, H. R. et al., 2005: Application of nonlinear acoustic tomography for non-destructive testing of trees. 14th International Symposium on Nondestructive Testing of Wood. Pp 337-349
7. Noack, D., Roth, W., 1976: On the theory of Elasticity of the orthotropic material wood. Wood Science and Technology 10: 97-110
8. Payton, R. G., 2003: Wave fronts in wood. Quarterly Journal of Mechanics and Applied Mathematics 56: 527-546
9. Rose, Joseph L., 1999: Ultrasonic Waves in Solid Media. Cambridge University Press
10. Schubert, S. et al., 2006: Rolling shear modulus and damping factor of spruce and decayed spruce estimated by modal analysis. Holzforschung 60: 78-84
11. Socco, L. V. et al., 2004: Feasibility of ultrasonic tomography for nondestructive testing of decay on living trees. Research in Nondestructive Evaluation 15(1): 31-54
12. Yee, K.S., 1966: Numerical Solution of Initial Boundary Value Problems Involving Maxwell's Equations in Isotropic Media. IEEE Transactions on Antennas and Propagation 14(3): 302-307
13. Zhang, H. et al., 2003: Automatic P-Wave Arrival Detection an Picking with Multiscale Wavelet Analysis for Single-Component Recordings. Bulletin of the Seismological Society of America 93(5): 1904-1912

Sandy Schubert
Swiss Federal Institute of Technology
ETH-Zentrum
HGF 21.3
CH-8092 Zürich
Switzerland
E-mail: niemz@fowi.ethz.ch

Empa
Überlandstr. 129
CH-8600 Dübendorf
Tel.: 41 448234028
E-mail: sandy.schubert@empa.ch

Daniel Gsell
Empa
Switzerland

Jürg Dual
Swiss Federal Institute of Technology
ETH-Zentrum
HGF 21.3
CH-8092 Zürich
Switzerland

Masoud Motavalli
Empa
Switzerland

Peter Niemz
Swiss Federal Institute of Technology
ETH-Zentrum
HGF 21.3
CH-8092 Zürich
Switzerland